Bioactive Materials 4 (2019) 224–235

Contents lists available at ScienceDirect

Bioactive Materials

journal homepage: http://www.keaipublishing.com/biomat

Modification of titanium surface via Ag-, Sr- and Si-containing micro-arc calcium phosphate coating

Mariya B. Sedelnikova[a,*], Ekaterina G. Komarova[a], Yurii P. Sharkeev[a,b], Anna V. Ugodchikova[b], Tatiana V. Tolkacheva[a], Julietta V. Rau[c], Evgeny E. Buyko[b,d], Vladimir V. Ivanov[d], Vladimir V. Sheikin[d]

[a] Institute of Strength Physics and Materials Science of SB RAS, Academicheskii Prospect 2/4, Tomsk, 634055, Russia
[b] National Research Tomsk Polytechnic University, Lenina Prospect 30, Tomsk, 634050, Russia
[c] Istituto di Struttura della Materia, Consiglio Nazionale delle Ricerche (ISM-CNR), Via del Fosso del Cavaliere 100, 00133 Roma, Italy
[d] Siberian State Medical University, Moscovskii Tract 2, Tomsk, 634050, Russia

ARTICLE INFO

Keywords:
Trace elements
Biocoatings
Micro-arc oxidation
Titanium substrate
Antibacterial activity

ABSTRACT

The current research is devoted to the study of the modification of the titanium implants by the micro-arc oxidation with bioactive calcium phosphate coatings containing Ag or Sr and Si elements. The coatings' microstructure, phase composition, morphology, physicochemical and biological properties were examined by scanning electron microscopy (SEM), transmission electron microscopy (TEM), energy-dispersive X-ray spectroscopy (EDX) and X-ray diffraction (XRD). Ag-containing and Sr-Si-incorporated coatings were formed in alkaline and acid electrolytes, respectively. The formation of the coatings occurred at different ranges of the applied voltages, which led to the significant difference in the coatings properties. The trace elements Ag, Sr and Si participated intensively in the plasma-chemical reactions of the micro-arc coatings formation. Ag-containing coatings demonstrated strong antibacterial effect against *Staphylococcus aureus* ATCC 6538-P. MTT *in vitro* test with 3T3-L1 fibroblasts showed no cytotoxicity appearance on Sr-Si-incorporated coatings.

1. Introduction

In the modern world, the requirements for biomedical materials have been increasing. Implants have to meet certain requirements, and therefore increase the quality and life expectancy of millions of people. For instance, implant materials have to correspond to certain physical, chemical and mechanical properties. What is more, they have to be biocompatible with surrounding tissues, namely they should not be the cause of allergic and/or inflammatory reactions in the body [1,2].

Artificial materials such as metals, polymers, ceramics, and bioactive glasses are successfully used to remove bone defects and restore bone tissue in traumatology, orthopedics and dentistry [3–5]. The most preferred materials in the surgery area are metals and alloys due to their strength, a combination of high mechanical properties and durability [6]. Cobalt-chromium and stainless steel alloys are well-known and have been used for many years as medical devises and implants. Cobalt-chromium alloys have excellent corrosion resistance, as well as biocompatibility. The main limitation of their use is the ability to disintegrate under long mechanical effects (friction, erosion, etc.) [7–9]. Stainless steel alloys are characterized by high strength and low cost, for example, compared to cobalt-chromium and titanium alloys. However, their prolonged implantation in the biological media can lead to the corrosion and releasing toxic metal ions such as iron and nickel into the surround tissues. Consequently, there is a disruption of the implant integrity and inflammatory reactions in the area of implantation [10–12].

Among all metal materials, titanium (Ti) and its alloys exhibit the best biological compatibility, excellent corrosion resistance, non-toxicity and a much lower elastic modulus compared to stainless steel and cobalt-chromium alloys (the elastic modulus of stainless steel is 200 GPa, cobalt-chromium alloys – 210 GPa, titanium – 110 GPa) [13–15]. Although Ti and its alloys are biocompatible, unfortunately, they are bioinert materials [16,17], hence they do not create conditions for osteointegration with bone tissue. Therefore, it is very promising to

Peer review under responsibility of KeAi Communications Co., Ltd.
* Corresponding author.
E-mail addresses: smasha5@yandex.ru (M.B. Sedelnikova), katerina@ispms.tsc.ru (E.G. Komarova), sharkeev@ispms.tsc.ru (Y.P. Sharkeev), ugodch99@gmail.com (A.V. Ugodchikova), tolkacheva@ispms.tsc.ru (T.V. Tolkacheva), giulietta.rau@ism.cnr.it (J.V. Rau), buykoevgen@yandex.ru (E.E. Buyko), ivanovvv1953@gmail.com (V.V. Ivanov), tsws@ssmu.ru (V.V. Sheikin).

https://doi.org/10.1016/j.bioactmat.2019.07.001
Received 7 May 2019; Received in revised form 1 July 2019; Accepted 16 July 2019
Available online 02 August 2019

create biocomposite materials which are able to combine a metal base and a bioceramic coating containing calcium phosphates (CP). By combining these materials, it is possible to produce an implant with excellent physical, mechanical and biological properties [18,19]. It is known that CP compounds are a part of inorganic components of bones, teeth and enamel [20]. Nowadays such CP compounds as monetite ($CaHPO_4$), brushite ($CaHPO_4{\cdot}2H_2O$), α- and β-tricalcium phosphate (α- and β-TCP, α- and β-$Ca_3(PO_4)_2$); hydroxyapatite (HA, $Ca_{10}(PO_4)_6(OH)_2$) are being under study [21–24]. HA and β-TCP are the preferred materials, owing to their lower solubility and Ca/P ratio of 1.67 and 1.5, respectively [25].

There are many ways to form the CaP biocoatings. The most popular methods are plasma deposition [26,27], biomimetic [28], sol-gel [29,30] and high-frequency magnetron sputtering [31,32]. Among the above mentioned methods of the coating deposition, the micro-arc oxidation (MAO) is one of the most effective methods owing to its high efficiency and low cost. A key feature of the process is the plasma discharge that occurs at the metal/electrolyte interface. When the applied voltage exceeds a certain critical value of the breakdown a series of discrete, short-lived micro-discharges appear. The micro-discharges move along the surface of the metal. As a result, a porous coating is formed [33–35].

Postoperative infections provoke a lot of problems in orthopedic surgery. *Staphylococcus aureus* bacteria have become resistant to antibiotics, so bioactive coatings with the addition of antimicrobial reagents can be an effective way to prevent infections [36,37]. Materials with special properties can be obtained by isomorphic substitutions in the structure of calcium phosphates such as HA and TCP. Metal ions (Ag^+, Cu^{2+} and Zn^{2+}) are widely used in medicine as antibacterial agents. Silver ions show particularly high antimicrobial activity [38,39]. Sufficiently small concentrations of silver in the range of 1.0–3.5 at% maintains low toxicity and high antimicrobial effect [40,41]. Nevertheless, a lot of publications concerned with the formation of Ag-containing HA show that it is rather difficult to obtain a single-phase product. As a rule, researchers get hydroxyapatite and silver particles [42]. Silver nanoparticles are reported to be cytotoxic because of the burst release of Ag ions [43]. In the present work, the possibility of the HA formation in micro-arc coatings during plasma-chemical reactions with the participation of silver ions which are embedded in the coating structure is shown.

As it has been indicated, strontium (Sr), which is natural bone-seeking trace element, enhances the osteoblast differentiation and bone matrix mineralization [44]. At the same time, Sr can inhibit bone resorption by reducing the osteoclast differentiation and resorption activity, and therefore it can induce osteoclast apoptosis [44,45]. Silicon (Si) is essential trace element in biological processes and it plays a specific metabolic role in bone growths [46]. The presence of Si at the surface of biomaterials may also enhance osteogenesis through a direct chemical mechanism and positively affect bone in-growth, osteogenesis, cell differentiation, and remodeling. Double substitutions in the structure of HA are very interesting. There are many publications showing the possibility of Sr-HA or Si-HA production. However, the obtaining of micro-arc coatings using HA with simultaneous replacement of Sr and Si was demonstrated in the present work for the first time. In this case, Sr and Si can enhance their osteogenic properties. Taking into consideration the beneficial effects of Sr and Si in the bone tissue, they can be used as doped element into CP biocoatings via MAO method.

The purpose of this research was to produce the micro-arc Ag- and Sr-Si-containing CP coatings on Ti substrate and to study their microstructure, phase composition, morphology, physicochemical and biological properties. In addition, a comparative study and analysis of the formation of micro-arc coatings in acidic and alkaline electrolytes was carried out.

2. Materials and methods

2.1. Sample preparation

Substrates from commercially pure titanium (99.58 Ti, 0.12 O, 0.18 Fe, 0.07C, 0.04 N, 0.01H wt%) were used for coatings deposition. Titanium plates 10 × 10 × 1 mm^3 in size were prepared as it was described in Ref. [2].

In order to carry out the MAO method the Micro-arc 3.0 technique was developed [2]. The installation consisted of a pulsed power source, a computer for controlling the deposition process, galvanic bath with water cooling system and two Mo electrodes.

Four types of the MAO coatings (CP-1, Ag-CP, CP-2 and Sr-Si-CP) depending on the electrolyte composition were obtained. It should be noted that CP-1 and Ag-CP coatings were deposited in the alkaline electrolyte (pH = 10–11), while CP-2 and Sr-Si-CP coatings were formed in the acid electrolyte (pH = 1–2). To produce the first type of coating (CP-1) the alkaline electrolyte containing Na_2HPO_4, NaOH, and β-$Ca_3(PO_4)_2$ was prepared. To synthesize the second type of coating (Ag-CP) silver nitrate $AgNO_3$ was added to the alkaline electrolyte in amount of 1 g/l. The third type of coating (CP-2) was produced in the acid electrolyte containing: 30% H_3PO_4, $CaCO_3$ and stoichiometric HA nano-powder. The fourth type of coating (Sr-Si-CP) was deposited in the acid electrolyte based on 30% H_3PO_4, $CaCO_3$ and Sr-Si-substituted HA ($Ca_{9.5}Sr_{0.5}(PO_4)_{5.5}(SiO_4)_{0.5}(OH)_2$). All types of the coatings were formed in the anodic potentiostatic regime for 5–10 min at the applied voltages of 200–450 V. Pulse frequency was of 50 Hz, pulse duration was of 100 μs.

2.2. Experimental methods

Morphology and microstructure of the coatings were examined by scanning electron microscopy (SEM, Zeiss LEO EVO 50, Germany) and transmission electron microscopy (TEM, JEOL JEM–2100, Japan) in "Nanotech" center at ISPMS SB RAS. Furthermore, the elemental composition and distribution of the elements in the coatings were also analyzed using energy-dispersive X-ray spectroscopy (EDX, INCA, Oxford Instruments) in combination with the SEM systems. The phase composition was determined with the help of X-ray diffraction analysis (XRD, DRON–7 "Nanotech" center) in the angular range of 2θ = 10–95° with a scan step of 0.02° with Co Kα radiation. The surface roughness was estimated with a Hommel–Etamic T1000 profilometer (Jenoptik, Germany) by the average roughness (Ra). The traverse length and rate of the measured profile were 6 mm and 0.5 mm/s, respectively. The coating thickness was determined with SEM cross-sectional micrographs.

The study of the coatings wettability was carried out by means of the installation of the Easy Drop DSA1 (Kruss, Germany). The contact angles were measured along the profile of a lying drop by tangent at the point of a three-phase solid-liquid-gas contact. To determine the free surface energy of the coatings the contact angles with both water (polar) and glycerol (non-polar) liquids were measured. The values of the surface tension of water and glycerol are 72.8 and 63.4 mN/m respectively. The calculation of the free surface energy of the coatings was performed according to the Owens-Wendt equation [47]:

$$\sigma_L(\cos\theta + 1) = 2\sqrt{\sigma_S^P \sigma_L^P} + 2\sqrt{\sigma_S^D \sigma_L^D}, \quad (1)$$

where σ_L^D, σ_S^D, σ_L^P, and σ_S^P are the dispersion and polar components of the free surface energy of the liquid and solid phases, and σ_L is the free surface energy of the test liquid.

2.3. Biological studies

The experiments *in vitro* with the pathogenic strain *Staphylococcus aureus* ATCC 6538-P (*S. aureus*) (the collection of the Department of

Microbiology of Siberian State Medical University, Tomsk, Russia) were performed to analyze the antibacterial activity of the Ag-CP coatings. The coating extracts were obtained by the sample incubation in 0.9% NaCl solution for 7 days at 37 °C (2 mL medium per sample was used according to ISO 10993-5). A microbial suspension with an extract (250 microbial bodies) was prepared in sterile conditions in 15 mL plastic tubes at proportion 1:1 (0.5 mL: 0.5 mL) and was incubated for 2 h at 37 °C. Then 0.4 mL of the suspension was placed on a nutrient agar medium (PAS) in Petri dishes and was cultured for 24 h at 37 °C and 100% humidity. The three types of samples group were used for comparison study of antibacterial activity. The first group (the control sample) was medium 0.9% NaCl solution (without coated plates), the second group was plates with calcium-phosphate coatings (CP-1) (without Ag) and the third group was plates with Ag-CP coatings. Three Petri dishes were taken for each group. The amount of *S. aureus* colony forming units (CFU) per cm^2 grown on PAS was calculated. The antibacterial activity against *S. aureus* was represented by the antibacterial rate (Z, %), following [42]:

$$Z = \frac{B - A}{B} \cdot 100\%$$

where A is the average number of bacteria on the tested sample, B is the average number of bacteria on the control sample. Each experiment was performed five times.

3T3-L1 mouse fibroblast culture (ATCC CL-173) [48] was used for *in vitro* cytotoxic tests of the coatings. The studies were carried out according to the MTT assay by standard ISO 10993–5–2009 [49]. Direct contact and extraction methods were used for the cell viability evaluation. In the study of viability by the contact method, the cells were planted in 6-well plates ("SPL lifescience", Korea). The cell density was 10^4 cells/cm^2 and their cultivation was carried out in complete DMEM/F12 nutrient medium with 10% fetal bovine serum (FBS). After the cells formation of 100% confluent monolayer, the test samples were placed in the wells. After 48 h of incubation, the cells were removed from the surface of the wells with a solution of trypsin-EDTA (0.25%) (PanEco, Russia) and their viability was determined.

The coating extracts were obtained by their incubation in DMEM/F12 culture medium at 37 °C for 72 h. Then the extracts were added to the wells after the cell formation of sub-confluent monolayer. The plates were incubated for 48 h at 37 °C in a CO_2-incubator MCO-5AS (SANYO, Japan) in an atmosphere of 95% air and 5% CO_2 [50]. The cells were precipitated by centrifugation. Then 1.5 mL DMSO (PanEco, Russia) was added to the sludge to dissolve the formazan. The amount of formazan was measured by means of an SF-2000 spectrophotometer (OKB-Spectr, Russia) at a wavelength of 560 nm. The results were analyzed using Statistics 10.0 software. The data has been seen as the mean, standard derivation and standard error of the mean, as well as the median (Me), 25% quartile (Q1) and 75% quartile (Q3). In order to analyze the available data sets a normal distribution Kolmogorov–Smirnov test was applied. The non–parametric Mann–Whitney's U–test was performed, and the differences of values at $p < 0.05$ were considered significant.

3. Results and discussion

3.1. Processes of CP, Ag- and Sr-Si- containing CP coatings formation by the MAO method in

Complicated plasma-chemical and electrochemical processes took place in the area of micro-arc discharges during the MAO process. As a result, the formation and growth of the coating layer occurred [13]. The dependences of the formed coatings' thickness as well as their roughness on the MAO physical parameters such as current density, deposition time and applied voltage have been revealed. In addition, the influence of the composition of the electrolyte on the thickness and roughness of the coating was identified. As shown in Fig. 1a (curve 1), the current density decreased during the MAO process owing to the growth of the coating layer with low electrical conductivity. Two stages can be distinguished in the growth mechanism of the coating.

The current density decreased according to the exponential law more intensively from 0.25 to 0.075 A/cm^2 at the first stage (up to ~ 3 min). In this case, the coating grew rapidly because of the occurrence of numerous intensive micro-arc discharges. During the second stage (from 3 to 10 min), the current density decreased to the minimum value as the coating became rather thick and prevented its breakdown. Micro-arc discharges died out.

The inverse exponential dependence of the Sr-Si-CP coating thickness growth at applied voltage of 200 V is observed in Fig. 1a (curve 2). The intensive growth of the coating thickness up to 30 μm occurred at the first stage. Then at the second stage, the growth rate slowed down, and the coating thickness increased by 20 μm. Another regularity of the MAO current density and coating thickness against the deposition time is observed in Fig. 1b for Ag-CP coatings. The current density decreased linearly from 0.8 to 0.2 A/cm^2 within the first minute of the coatings deposition. For the following 2 min, current density decreased gradually to the minimum value, and, after that, remained constant. In this case the coating thickness increased linearly up to 54 μm.

It was found out that the formation of the coatings in different electrolytes occurred under the different applied voltages (Fig. 1c and d). The thickness and roughness of the CP-1 and Ag-CP coatings deposited in the alkaline electrolytes increased from 20 to 50 μm (Fig. 1c, graphs 3,4) and from 1.5 to 4.0 μm (Fig. 1d, graphs 3,4), respectively, with increasing of the MAO voltage from 350 to 450 V. Meanwhile, the CP-2 and Sr-Si-CP coatings formed in the acid electrolytes at voltages of 200–350 V were characterized by the significantly greater thickness and roughness as compared to the coatings produced in the alkaline electrolytes. Their thickness and roughness increased intensively from 30 to 140 μm (Fig. 1c, graphs 1,2) and from 2 to 8 μm (Fig. 1d, graphs 1,2) respectively, with increasing of the applied voltage. According to the researchers [51], the range of value of the surface roughness from 2.0 to 3.0 μm is optimal since the surfaces with this roughness are the most suitable for the bone tissue regeneration.

It should be emphasized that the value of thickness and roughness for CP-1 and CP-2 coatings without trace elements was lower than that for Ag-CP and Sr-Si-CP coatings. Thus, trace elements participated in the plasma-chemical reactions during the MAO process and intensified them. The compositions and properties of the obtained coatings are presented in Table 1.

3.2. Characterization of the CP-1 and Ag-CP macro-arc coatings formed in the alkaline electrolyte

SEM studies showed the presence of the developed surface morphology and porous structure in the CP-1 and Ag-CP coatings (Fig. 2). A large number of isometric particles uniformly distributed over the coating surface and can be seen in SEM-images (Fig. 2 a-d). These particles correspond to β-TCP transferred from the electrolyte into the coating surface during the MAO process [23].

Numerous ridges and hollows were observed in SEM images of the coatings formed at higher voltage of 450 V (Fig. 2 c,d). They were formed under the action of powerful local micro-arc discharges. In addition, as the applied voltage increased from 350 to 450 V, the average pore size grew from 1.7 to 3.7 μm (Fig. 3). The SEM images of the coatings cross-section demonstrated their internal porous structure (Fig. 2 e,f).

Fig. 3 shows the histograms of the pore size distribution in the coatings depending on the applied voltage and electrolyte composition. All histograms had unimodal distribution. It was found, that the average pore size increased not only with an increase in the applied voltage, but also with the introduction of silver ions into the electrolyte. Therefore, it confirmed that the MAO process occurred more intensively with the participation of silver ions.

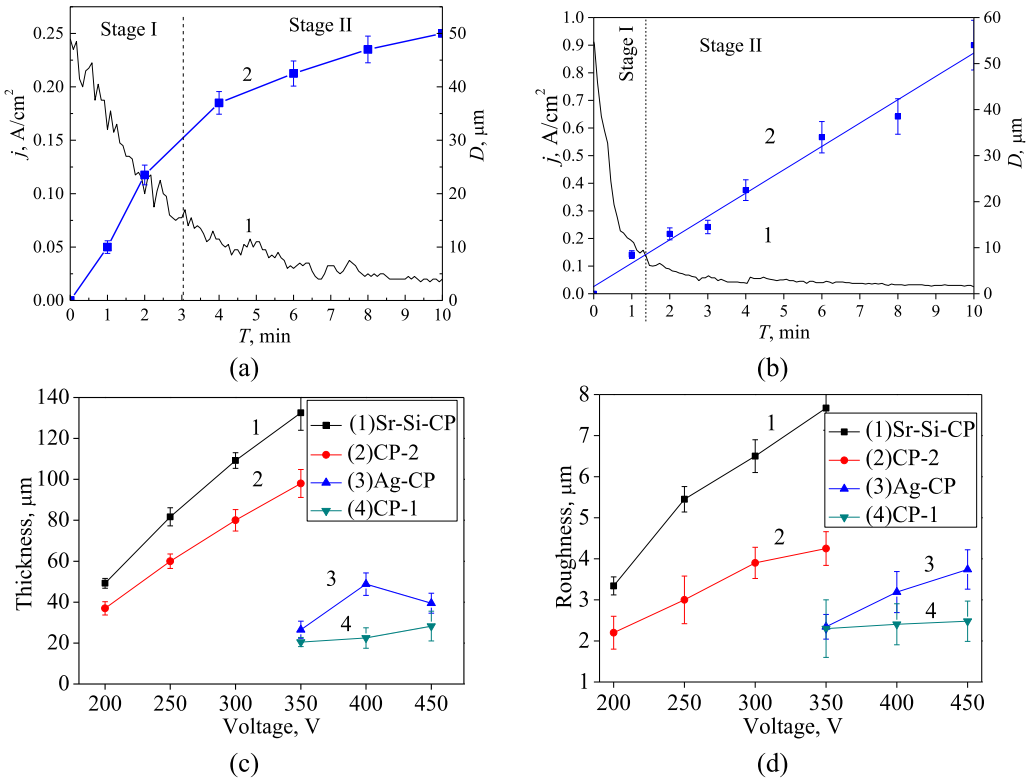

Fig. 1. Graphs of the MAO current density (a,b curve 1) and the coating thickness (a,b curve 2) against the MAO time for the deposition of Sr-Si-CP coatings at 200 V (a) and the deposition of Ag-CP coatings at 400 V (b). Graphs of the thickness (c) and surface roughness Ra (d) against the MAO voltage for all types of the coatings.

Table 1
Characteristics of the coatings.

Electrolyte	alkaline (pH = 10–11)		acid (pH = 1–2)	
Coating type	CP-1	Ag-CP	CaP-2	Sr-Si-CP
Voltage, V	350–450		200–350	
Thickness, μm	20–30	25–50	35–100	50–140
Roughness Ra, μm	1.5–2.5	1.5–4.0	2.0–4.5	3.0–8.0

The dependences of the hydrophilic properties of Ag-CP coatings on the applied voltage and the process duration were investigated (Fig. 4). It is known that hydrophilic surfaces exhibit high cell adhesion and proliferation, as well as protein adsorption [52]. Wettability studies of Ag-CP coatings showed that the values of the wetting angles with water and glycerol were in the range of 65–73° (Fig. 4 a). In the meantime, wetting angle with water for the Ag-CP coatings deposited for 10 min decreased linearly up to 48° when the process voltage increased up to 450 V.

The free surface energy of the Ag-CP coatings deposited for 10 min was calculated according to Owens-Wendt method (Eq. (1)) via two dispersion and polar components. It was revealed that the polar component predominated significantly and equals to ~33 mN/m (Fig. 4 b). Meanwhile, the dispersion component did not exceed 9 mN/m. This is due to the presence of the polar chemical bonds in the coatings. These polar bonds determine the value of the free surface energy that equals to 37–41 mN/m regardless of on the value of the applied voltage.

As a result of EDX analysis of the CP-1 and Ag-CP coatings the changes in the Ca/P ratio which depend on the applied voltage and electrolyte composition were established (Fig. 5). Varying the silver content in the Ag-CP coatings was also studied in this case.

The Ca/P ratio was determined in the whole area of the coatings (area 1 marked by the yellow line in Fig. 5a), in the local areas containing TCP particles (area 2) and in the local areas without any particles (area 3).

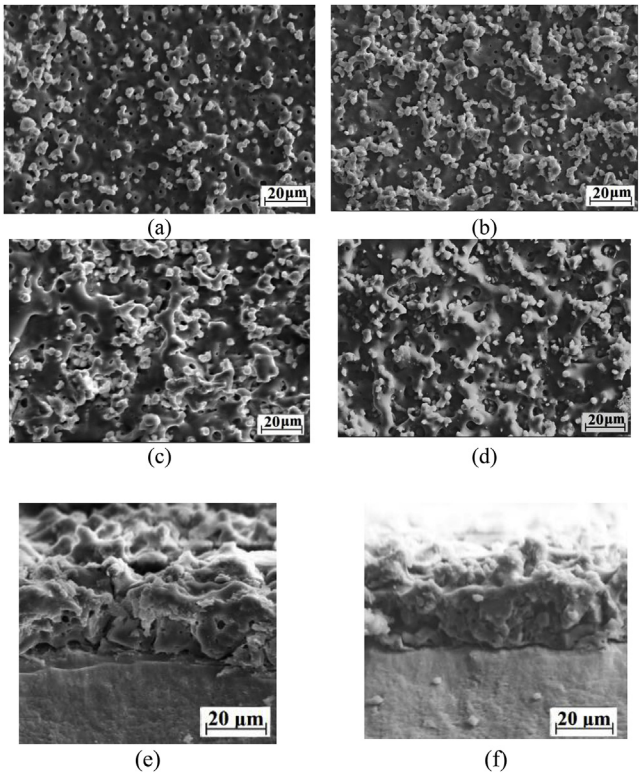

Fig. 2. SEM images of the surface (a–d) and cross-section (e, f) of the CP-1 (a, c) and Ag-CP (b, d) coatings deposited at 350 V (a, b) and 450 V (c–f) for 10 min.

The histograms showed that the Ca/P ratio in all the studied areas of both Ag-free coatings and Ag-containing coatings did not differ much and was 1.0–1.2 (Fig. 5c). The elements maps demonstrated uniform

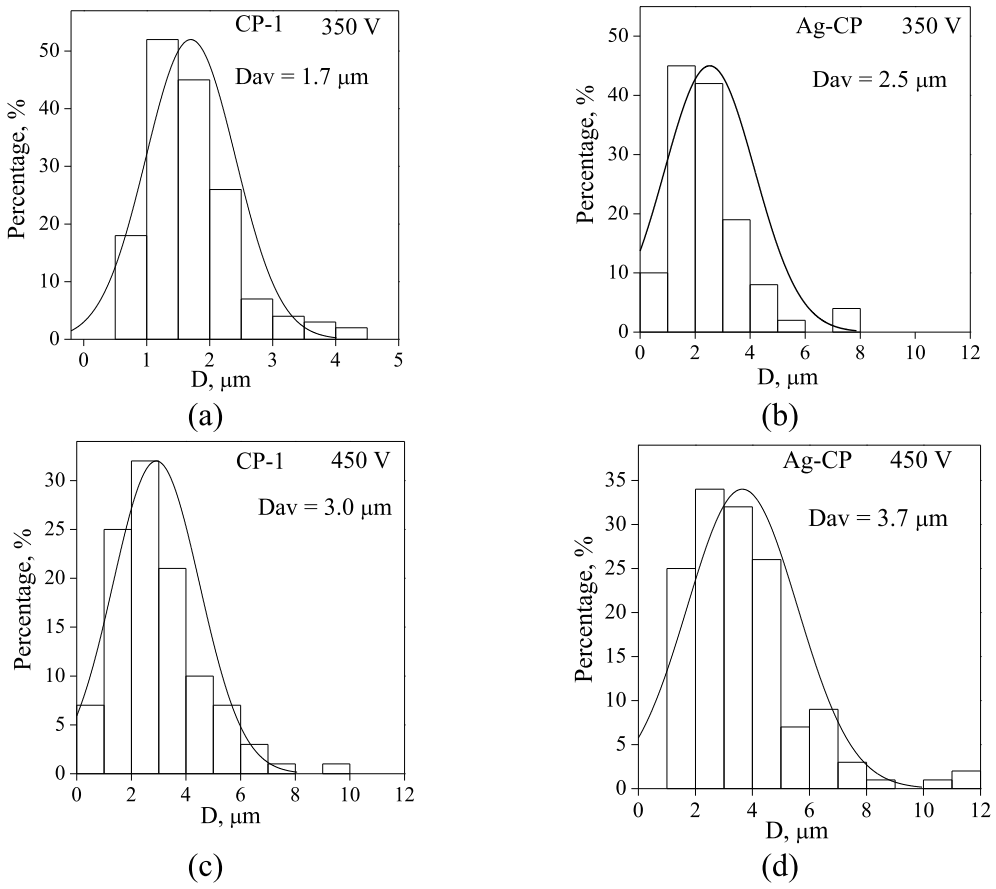

Fig. 3. Histograms of the pore distribution by sizes for CP-1 (a, c) and Ag-CP (b, d) coatings deposited on the Ti for 10 min.

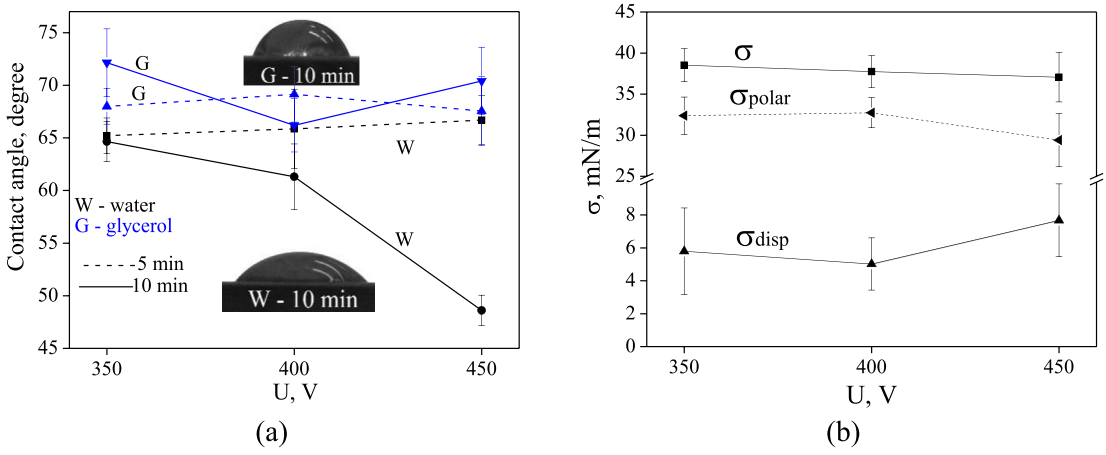

Fig. 4. Graphs of contact angles (a) with water (W) and glycerol (G), and free surface energy (b) of Ag-CP coatings against the applied voltage.

distribution of the elements, especially, of silver in the coatings (Fig. 5b). When the MAO process voltage increased from 350 to 450 V the silver content in the coatings grew from 0.3 to 0.8 at.% (Fig. 5d).

XRD study revealed the crystalline structure in the CP-1 and Ag-CP coatings (Fig. 6). The crystalline phases such as β-TCP, α-TCP and titanium oxide TiO_2 in the form of anatase were identified in the coatings. The oxide layer was formed in the coatings due to the oxidation of the substrate material. β-TCP transferred from the electrolyte to the coating at the last moment of deposition, when the current density becomes minimal (Fig. 1a). Polymorphic transformation of β-TCP in α-TCP took place because there was a high temperature above 1100 °C in the area of the micro-arc discharge.

It was found by TEM studies that additionally the phase of HA presented in the fragments of CP-1 and Ag-CP coatings besides the β-TCP, α-TCP and TiO_2 phases (Fig. 7). Crystallites of isometric shape and sizes from 20 to 170 nm were clearly visible on the dark-field TEM images of particles in the reflections (131) from β-TCP, (132) from α-TCP and (331) from HA. In this case the crystallites of HA and α-TCP were observed mainly on the particle borders. Thus, it is assumed that α-TCP and HA were formed in the surface layer of the coatings as a result of high-temperature reactions which happened in the process of micro-arc coatings synthesis. Moreover, the phase transition β-TCP in α-TCP and the formation of HA occurred at the interface of β-TCP particles.

The antibacterial activity of CP-1 and Ag-CP coatings deposited in the alkaline electrolyte at 450 V against *S. aureus* strain was determined

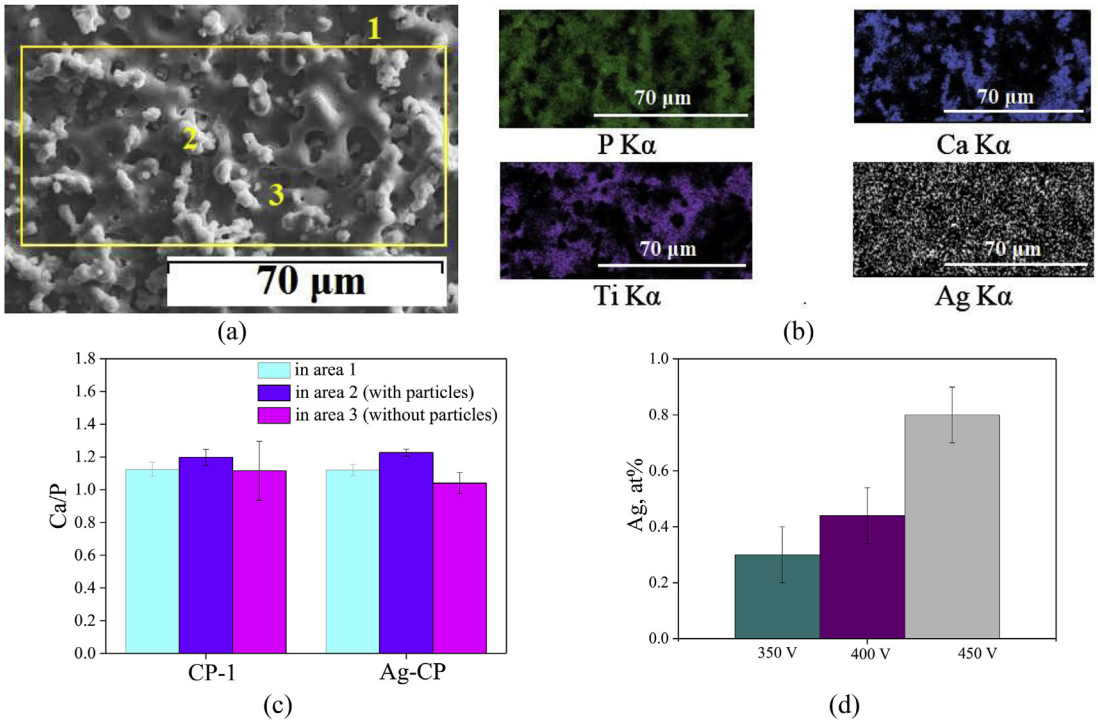

Fig. 5. SEM image of Ag-CP coating deposited at 450 V (a) and the elemental analysis results (b–d): elements maps distribution (b); diagrams of the Ca/P ratio (c) in the CP-1 and Ag-CP coatings; diagram of Ag content in Ag-CP coatings (d) against the applied voltage.

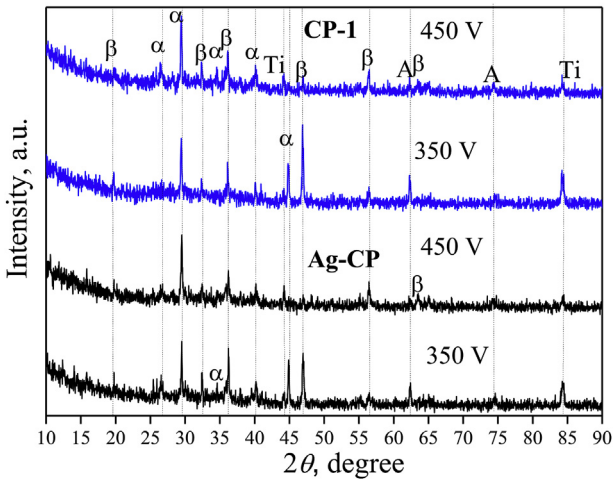

Fig. 6. XRD patterns of the CP-1 and Ag-CP coatings deposited for 10 min; α – α-TCP, β – β-TCP, A – TiO_2 (anatase), Ti – titanium.

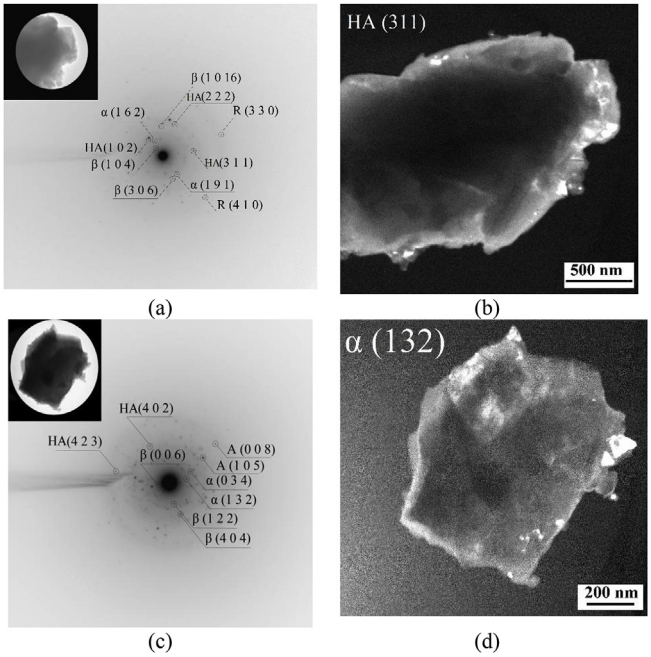

Fig. 7. The bright-field (a, c), dark-field (b, d) TEM images and SAD pattern (a, c) of the CP-1 (a, b) and Ag-CP (c, d) coatings deposited at 450 V; HA – hydroxyapatite, β – β-TCP, α – α-TCP, R – rutile, A – anatase.

(Fig. 8). The highest concentration of *S. aureus* CFU was found in the extracts of the CP-1 coatings (without silver). The number of *S. aureus* CFU reduced significantly in the extracts of the Ag-CP coatings. Therefore, the Ag-CP coatings were characterized by the high antibacterial rate against *S. aureus* which equals to 45%. The influence of Ag-CP coatings on the growth of microorganisms can be described as a bacteriostatic effect caused by suppression of the growth of microorganisms and a decrease in the number of CFU. Linling Yin et al. [43] performed a similar analysis, in which they demonstrated a coating with the layer of TiO_2 nanotubes doped with silver nanoparticles that exhibited antibacterial rate against planktonic *S. aureus* which equals to 37.4%.

As reported [34,36,43] Ag exhibit excellent antibacterial properties in broad spectrum of bacteria, including gram-positive and gram-negative bacteria. The antibacterial effect of Ag becomes apparent when it is dissolved in body fluids. In this case binding with proteins occurs, which, in its turn, leads to disturbance of the microbes' activity and the suppression of their proliferation. In the present work, the coatings were deposited in an electrolyte containing 1 g/l $AgNO_3$. The silver content in the coatings determined by the EDX method varied in the range of 0.3–0.8 at. %. Previous studies [53] showed that after the 5-week coatings dissolution the silver content halved, which indicates that silver dissolves in the biological media. But even after 24 h of

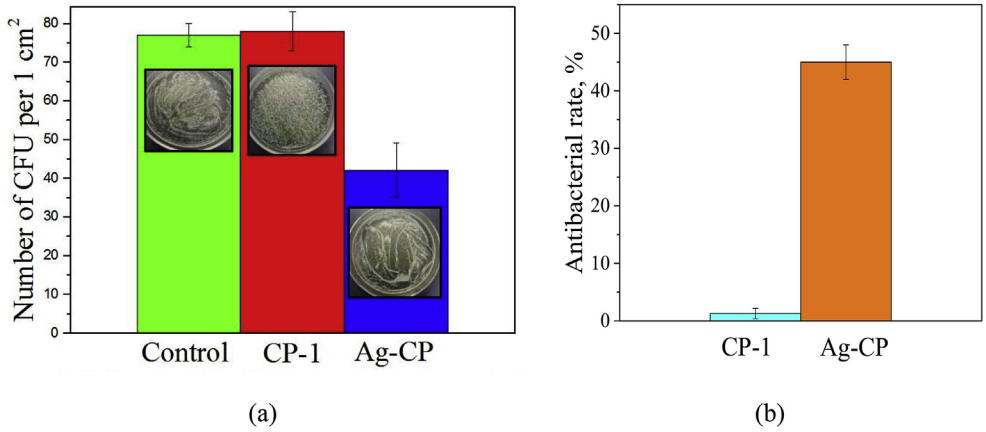

Fig. 8. 24-hour incubation of *S. aureus* in the coating extracts (a) and antibacterial rates of CP-1 and Ag-CP coatings against *S. aureus*

interaction of *S. aureus* with 7-day extracts of Ag-CP coatings, a clear bacteriostatic effect was observed as compared with medium of 0.9% NaCl and CP1 coatings.

But antibacterial activity of Ag coatings can be accompanied by a cytotoxic effect, as reported by M. Rizwan et al. [34]. The *in vitro* cytotoxic test of the CP-1 and Ag-CP biocoatings demonstrated that the number of viable cells after 24 h of cultivation in the direct contact with the coatings exceeded 89% (Table 2). Thus, it was found that the coatings did not show cytotoxic effect in the direct *in vitro* 24-h contact with cells.

3.3. Characterization of the CP-2 and Sr-Si-CP macro-arc coatings formed in the acid electrolyte

The performed study proved that CP-2 and Sr-Si-CP coatings were different from CP-1 and Ag-CP coatings not only in their thickness and roughness, but also in their surface morphology due to the different parameters of the coatings deposition and various compositions of the electrolytes. The surface morphology of the CP-2 and Sr-Si-CP coatings included the spheroidal elements and open pores (Fig. 9 a–c). The formation of spheres and pores in the coatings occurred owing to the gas-plasma "bubbles" generation in the channels of micro-arc discharges. A threadlike channel filled with plasma was formed in the coating layer [2]. The hole of the channel facing the electrolyte was the outlet for the heated substance. As the voltage increased in the range of 200–350 V, the intensity of micro-arc discharges also increased which consequently led to the temperature rise inside the channels. As the result, the sizes of the pores and spheres increased from 4.9 to 8.1 μm and from 17.0 to 29.2 μm, correspondingly (Fig. 10). The plate-like crystals were observed inside the spheres and hemispheres (Fig. 9 b,c). It was found earlier [23], that an increase of voltages above 400 V was accompanied by the transition of micro-arc discharges into arc ones and coatings destruction.

The complicated porous structure with a large number of round and elliptical pores was detected by observing of SEM images the coatings cross-sections (Fig. 9 d–f). As it has been illustrated, the coatings thickness and roughness increased linearly in the range of 30–140 μm and 2–8 μm, respectively, as the voltage increased (Fig. 1 c,d). In this case, large pores of almost 20 μm in diameter were formed (Fig. 9 e,f).

As X-ray analysis has shown, the structure of CP-2 and Sr-Si-CP coatings transformed with the voltage increasing (Fig. 11 a,b).

XRD patterns of the coatings deposited at 200 V demonstrated the diffuse halo in the angular range of $2\theta = 20–35^{\circ}$ so the coatings had an amorphous structure. Reflexes corresponding to the substrate material Ti were observed on the XRD pattern of the CP-2 coating deposited at the voltage of 200 V. This is due to fact that the CP-2 had lower thickness compared to Sr-Si-CaP (Fig. 1c). When the voltage increased in the range of 250–350 V, the diffraction reflexes of monetite ($CaHPO_4$) appeared on the XRD patterns, moreover, the intensity of reflexes from different crystallographic planes of $CaHPO_4$ increased. In this case the halo area expanded to $2\theta = 20–40^{\circ}$. Thus, with increasing of the applied voltage, the structure of the coatings became amorphous-crystalline wherein the content of the crystalline phase was equal to 35 ± 5 wt%.

The bright-field and dark-field TEM images and SAD patterns of the Sr-Si-CP coatings obtained at different applied voltages are illustrated in Fig. 12.

The TEM results confirmed that Sr-Si-CP coatings obtained at low voltage of 200 V had an amorphous microstructure. The SAD pattern contained up to four diffuse halos corresponding to amorphous calcium phosphate compounds (Fig. 12b). Increasing of the voltage up to 350 V led to the transformation of the coatings microstructure from amorphous to amorphous-crystalline. Numerous point-ring reflections together with diffuse halos were observed in SAD patterns of coatings deposited at 350 V (Fig. 12e). The indication of the SAD pattern proved the presence of the following phases in the coatings: α-$Ca_2P_2O_7$ with an orthorhombic lattice (JCPDS standard No. 09–0345); β-$Ca_2P_2O_7$ with a tetragonal lattice (JCPDS standard No. 09–0346); $CaHPO_4$ with triclinic lattice (JCPDS standard No. 09–0080), TiO_2 in anatase (JCPDS standard No. 21–1272) and rutile (JCPDS standard No. 21–1276) modifications with a tetragonal lattice. The crystallites from 5 to 80 nm in size and their agglomerates of up to 150 nm in size were observed on the dark-

Table 2
Results of *in vitro* cytotoxic test of CP-1 and Ag-CP coatings, Me (Q1 – Q3).

Groups, n = 5	Viable cells, % after 24-h cultivation, direct contact method
Cells without coating, control group	100
Cells with CP-1 coating,	98.9 (96.5–100.0)
Cells with Ag-CP coating	95.4 (89.0–100.0)

Note: The results are presented as the median (Me) characterizing values in 50% of samples, Q_1 – 25% percentile and Q_3 – 75% percentile. Differences compared with the controls by Mann-Whitney U–test were considered significant at $p < 0.05$, n – the number of tested specimens.

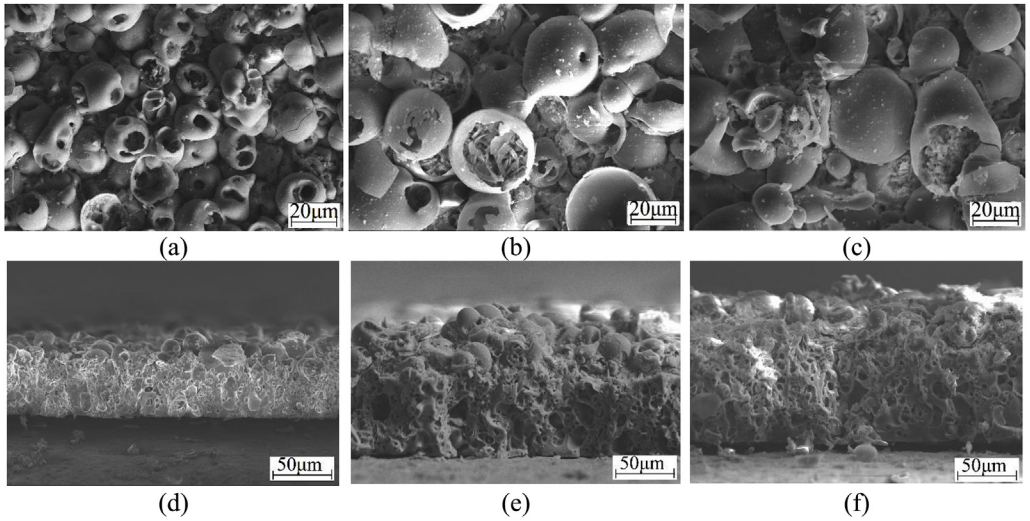

Fig. 9. SEM images of the surface (a–c) and cross-section (d–f) of the Sr-Si-CP coatings deposited on Ti for 10 min, at the following voltages: 200 V (a,d), 300 V (,e) and 350 V (c,f).

field TEM images in the reflections (201) α-$Ca_2P_2O_7$, (206) β-$Ca_2P_2O_7$ and $CaHPO_4$ (Fig. 12 f–h). The form of all crystallites was close to equiaxial.

The amount of elements determined by the EDX microanalysis in Sr-Si-CP coatings deposited at the different voltages is presented in Table 3. When the applied voltage increased the concentration of Ca increased too, while P and Ti concentration decreased. In this case, the amount of Sr and Si remained unchanged. The growth of the applied voltage led to an increase in the intensity of micro-arc discharges and an increase in the temperature of the electrolyte. Therefore, the dissolution of hydroxyapatite and the interaction of calcium phosphate substances with the substrate occurred more intensively. Crystalline compounds such as $Ca_2P_2O_7$ and $CaHPO_4$ were formed in the coatings so the Ca/P ratio grew from 0.3 to 0.5.

The maps of the elements distribution showed that Ti, P, Ca, Sr, and Si were distributed evenly on the surface of Sr-Si-CP coatings deposited at applied voltage of 200 V. However, in the coatings obtained at the voltage of 350 V, calcium and phosphorus were localized in the areas of

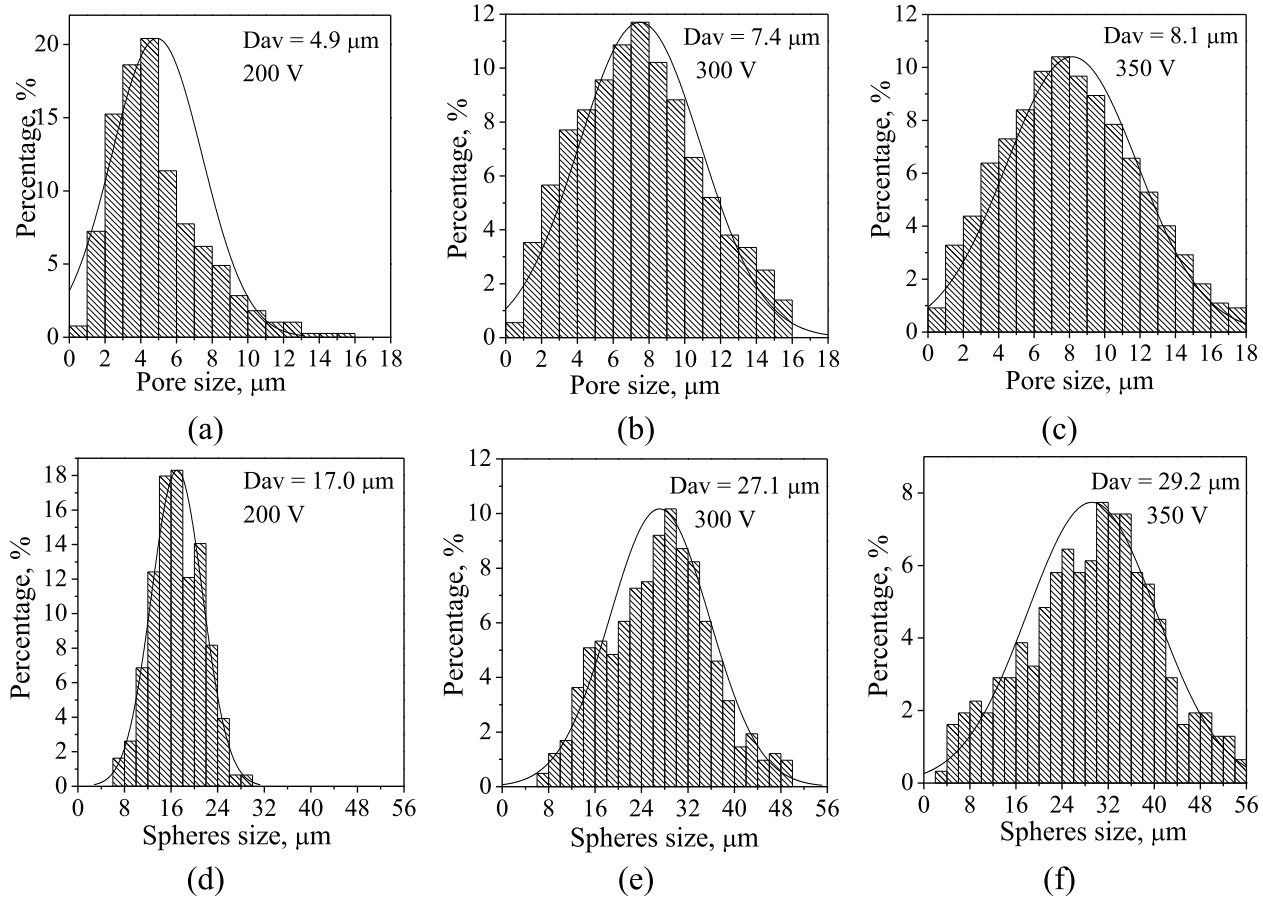

Fig. 10. Histograms of distribution of the pores (a–c) and spheres (d–f) by sizes in the Sr-Si-CP coatings deposited at the different applied voltages.

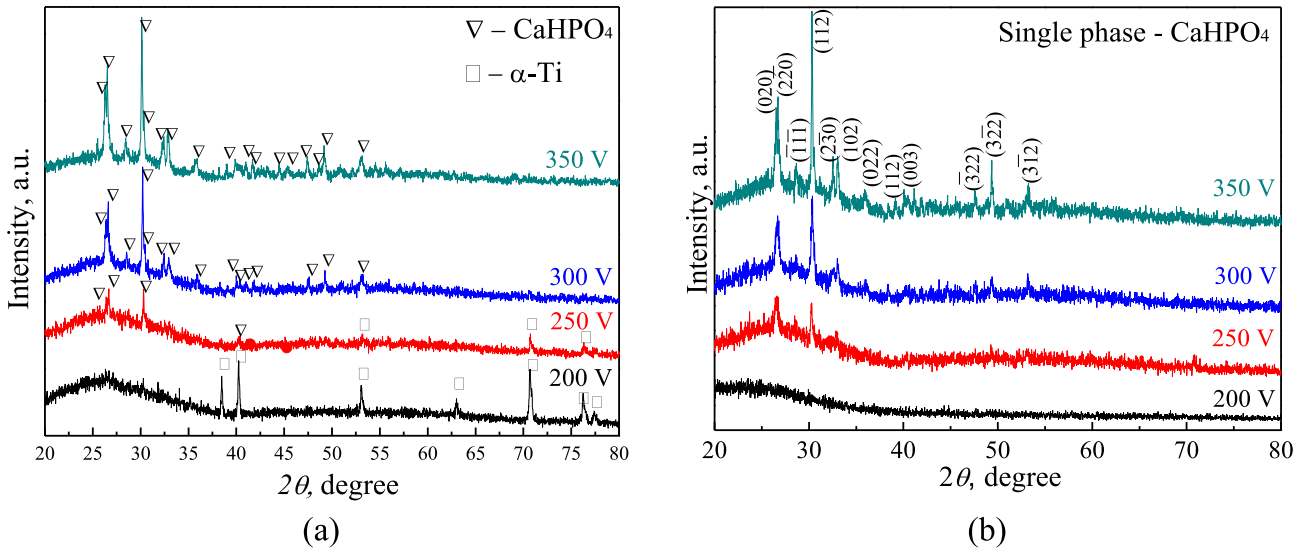

Fig. 11. XRD patterns of CP-2 (a) and Sr-Si-CaP (b) coatings deposited at different applied voltages.

plate crystals (Fig. 13).

Biological *in vitro* MTT test of the CP2 and Sr-Si-CP biocoatings demonstrated that the fraction of viable 3T3-L1 fibroblasts after 48 h of cultivation in the direct contact with the CP-2 coatings and in their extracts was more than 86% (Table 4). In the case of cultivation of cells with Sr-Si-CaP coatings, a decrease in cell viability was not observed, and their proliferative activity increased (108–113%). This is the evidence of the high biocompatibility of the CP-2 and Sr-Si-CP coatings and the absence of cytotoxic impact on the cells. This result can imply the osseoconductive and osteotropic properties of the Sr-Si-CP biocoatings.

The amount of evidence that Sr enhances bone remodeling has increased [54]. Partial calcium substitution by strontium in hydroxyapatite structure could increase bone formation and, what is more, decrease bone resorption. This leads to the prevention of bone loss and increases bone mass and bone strength. Besides, Sr may enhance

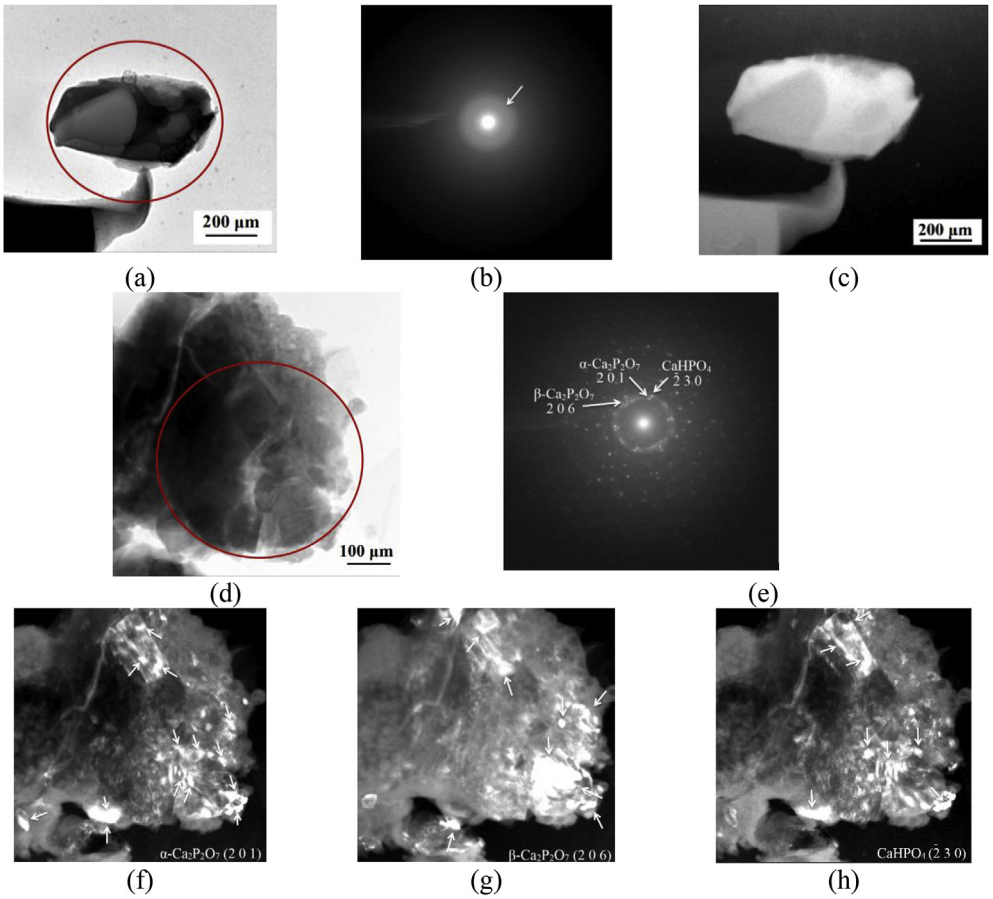

Fig. 12. Light-field (a, d) and dark-field (c, f–h) TEM images and SAD pattern (b, e) of the. Sr-Si-CP coatings deposited at the following voltages: 200 V (a–c), 350 V (f–h). SAD patterns were obtained from the marked round areas.

Table 3
Elemental composition of Sr-Si-CaP coatings.

Elements	Number of the elements on the coating surface, at.%		
	200 V	300 V	350 V
Ca	5.4 ± 0.2	8.0 ± 0.5	9.1 ± 0.5
P	20.7 ± 0.3	19.7 ± 0.6	18.9 ± 0.2
O	59.4 ± 0.4	60.3 ± 1.5	61.9 ± 0.5
Ti	13.3 ± 0.5	10.6 ± 1.3	8.8 ± 0.8
Sr	0.8 ± 0.1	0.8 ± 0.1	0.8 ± 0.1
Si	0.5 ± 0.1	0.6 ± 0.1	0.6 ± 0.1
Ca/P	0.3	0.4	0.5

calcified matrix formation by stabilizing hydroxyapatite (HA) crystals.

Dandan Hu et al. reported [55] that Sr^{2+} substitution for Ca^{2+} in plasma sprayed calcium silicate (Ca–Si) coatings decreased their bioresorption in biological media and improved their biological performance. By incorporating Sr^{2+} the mineralized nodules on the Sr-$CaSiO_3$ coating were able to be modulated more beneficially because of the accelerated biomineralization. Thus, the Sr and Si presence locally at the interface between the implant and bone via a calcium phosphate coating should stimulate bone formation and enhance osteointegration.

4. Conclusions

Bioactive Ag or Sr-Si-containing CP coatings were produced by the MAO method. To synthesize Sr-Si-incorporated coatings the acid electrolyte was used, and to form Ag-containing coatings the alkaline electrolyte was used. The formation of the coatings took place at different applied voltages, and the coatings properties varied significantly. The Sr-Si-CP coating thickness increased exponentially with MAO time, while the Ag-CP coating thickness increased linearly.

Table 4
Viability of 3T3-L1 cells cultivated in the direct contact with the coatings and in their extracts in DMEM/F12 media for 48 h, Me(Q_1 – Q_3).

Groups, n = 3	Percentage of viable cells, %	
	Direct contact method	Extract method
Cells without coating, control group	100	100
Cells with CP-2 coating	86.2 (83.7–95.4)	117.9 (107.9–131.4)
Cells with Sr-Si-CP coating	108.1 (104.7–117.2)	112.9 (107.7–118.9)

Note: The results are presented as the median (Me) characterizing values in 50% of samples, Q_1 – 25% percentile and Q_3 – 75% percentile. Differences compared with the controls by Mann-Whitney U–test were considered significant at $p < 0.05$, n – the number of tested specimens.

The values of thickness and roughness for the coatings without additive elements were lower than those for Ag-CP and La-Si-CP coatings. Thus, Ag, Sr and Si elements participated in the plasma-chemical reactions of the micro-arc coatings formation and intensified them.

The surface morphology of the coatings deposited into the alkaline and acid electrolytes was different. Ag-CP coatings contained pores and isometric particles of β-TCP uniformly distributed in the coatings. The spheroidal elements and open pores were observed on the surface of Sr-Si-CP coatings.

The phase composition of Ag-CP coatings included following crystalline phases: β-TCP; α-TCP; HA; TiO_2 (anatase, rutile). Sr-Si-CP coatings deposited at 200 V had amorphous structure. When the applied voltage increased up to 350 V, the coatings structure transformed from amorphous to amorphous-crystalline. Crystalline compounds such as $Ca_2P_2O_7$, $CaHPO_4$ and TiO_2 (anatase, rutile) were formed in this case.

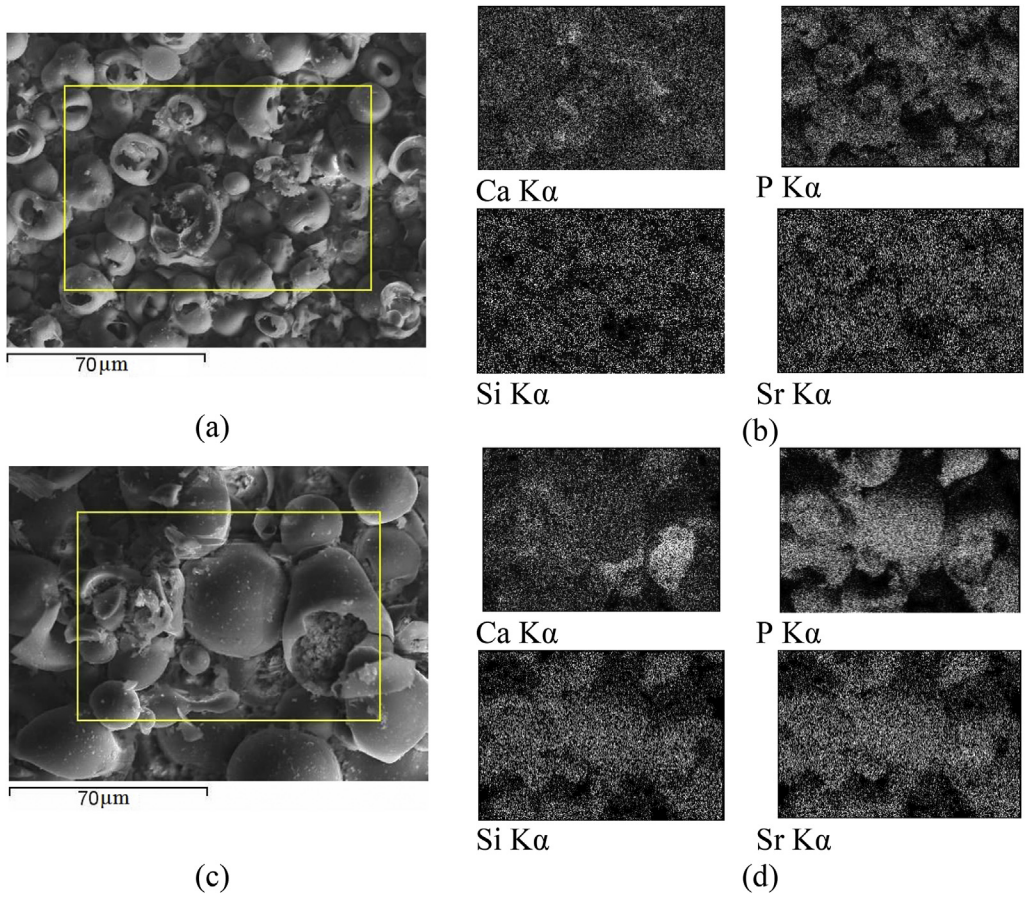

Fig. 13. SEM images (a, c) and elements maps distribution (b, d) of the Sr-Si-CP coatings deposited at the voltage of 200 V (a, b) and 350 V (c, d).

Ag-CP coatings demonstrated strong bacteriostatic effect against *S. aureus*. At the same time, as Ag-CP as Sr-Si-CP coatings did not show cytotoxic effect on the fibroblasts. Moreover Sr-Si-CP coatings increased cells proliferative activity. This result can imply the osseoconductive and osteotropic properties of the Sr-Si-CP biocoatings. The Sr and Si presence locally at the interface between the implant and bone via a calcium phosphate coating should stimulate bone formation and enhance osteointegration [55]. However, further research of the antibacterial and osteotropic properties of Ag-CP and Sr-Si-CP biocoatings for functionalization of the surface of metallic implants and biomedical application is also required.

Conflicts of interest

The authors declare no conflict of interest.

Acknowledgments

The work has been financially supported by the Fundamental Research Program of the State Academies of Sciences for 2013-2020, direction of research III.23.2. The authors express acknowledgements to Dr. M.V. Chaikina (ISSCM SB RAS, Novosibirsk, Russia), A.I. Tolmachev, P.V. Uvarkin, V.V. Chebodaeva, I. A. Glukhov and M. A. Khimich (ISPMS SB RAS, Tomsk, Russia) for their assistance in carrying out of the research.

References

[1] Y.-F. Ding, R.W. Li, M. Nakai, T. Majumdar, D.-H. Zhang, M. Niinomi, N. Birbilis, P.N. Smith, X.-B. Chen, Osteoanabolic implant materials for orthopedic treatment, J. Adv. Healthcare Mater. 5 (14) (2016) 1–13, https://doi.org/10.1002/adhm.201600074.

[2] S.V. Gnedenkov, Y.P. Sharkeev, S.L. Sinebryukhov, O.A. Khrisanfova, E.V. Legostaeva, A.G. Zavidnaya, A.V. Puz, I.A. Khlusov, D.P. Opra, Functional coatings formed on the titanium and magnesium alloys as implant materials by plasma electrolytic oxidation technology: fundamental principles and synthesis conditions, J. Corros Rev; aop. 34 (1–2) (2016) 1–19, https://doi.org/10.1515/corrrev-2015-0069.

[3] L. Li, M. Zhang, Y. Li, J. Zhao, L. Qin, Y. Lai, Corrosion and biocompatibility improvement of magnesium-based alloys as bone implant materials: a review, J. Regenerative Biomaterials 4 (2) (2017) 129–137, https://doi.org/10.1093/rb/rbx004.

[4] M. Saini, Y. Singh, P. Arora, V. Arora, K. Jain, Implant biomaterials: a comprehensive review, World Journal of Clinical Cases 3 (1) (2015) 52–57, https://doi.org/10.12998/wjcc.v3.i1.52.

[5] A. Revathi, A.D. Borrás, A.I. Muñoz, C. Richard, G. Manivasagam, Degradation mechanisms and future challenges of titanium and its alloys for dental implant applications in oral environment, Mater. Sci. Eng. C 76 (2017) 1354–1368, https://doi.org/10.1016/j.msec.2017.02.159.

[6] Y. Sua, C. Luoa, Z. Zhanga, H. Hermawanc, D. Zhue, J. Huanga, Y. Lianga, G. Lib, L. Ren, Bioinspired surface functionalization of metallic biomaterials, J. Mech. Behav. Biomed. Mater. 77 (2018) 90–105 https://doi.org/10.1016/j.jmbbm.2017.08.035.

[7] F. Mindivan, M.P. Yıldırım, F. Bayındır, H. Mindivan, Corrosion and tribocorrosion behavior of cast and machine milled Co-Cr alloys for biomedical applications, Acta Phys. Pol., A 129 (2015) 701–704, https://doi.org/10.12693/APhysPolA.129.701.

[8] A. Ozkomur, Y. Ucar, O. Ekren, R.S.A. Shinkai, E.R. Teixeira, Characterization of the interface between cast-to Co-Cr implant cylinders and cast Co-Cr alloys, J. Prosthet. Dent (2016) 1–9 https://doi.org/10.1016/j.prosdent.2015.07.021.

[9] G. Barucca, E. Santecchia, G. Majni, E. Girardin, E. Bassoli, L. Denti, A. Gatto, L. Iuliano, T. Moskalewicz, P. Mengucci, Structural characterization of biomedical Co–Cr–Mo components produced by direct metal laser sintering, Mater. Sci. Eng. C 48 (2015) 263–269 https://doi.org/10.1016/j.msec.2014.12.009.

[10] A.A. Oshkour, S. Pramanik, M. Mehrali, Y.H. Yau, F. Tarlochan, N.A. Abu Osman, Mechanical and physical behaviour of newly developed functionally graded materials and composites of stainless steel 316L with calcium silicate and hydroxyapatite, J. Mech. Behav. Biomed. Mater. 15 (2015) 321–331 https://doi.org/10.1016/j.jmbbm.2015.05.020.

[11] M. Cieślik, K. Engvall, J. Pan, A. Kotarba, Silane–parylene coating for improving corrosion resistance of stainless steel 316L implant material, Corros. Sci. 53 (2011) 296–301, https://doi.org/10.1016/j.corsci.2010.09.034.

[12] M. Kheirkhah, M. Fathi, H.R. Salimijazi, M. Razavi, Surface modification of stainless steel implants using nanostructured forsterite (Mg_2SiO_4) coating for biomaterial applications, Surf. Coat. Technol. 276 (2015) 580–586 https://doi.org/10.1016/j.surfcoat.2015.06.012.

[13] A. Krzakała, A. Kazek-Kesik, W. Simka, Application of plasma electrolytic oxidation to bioactive surface formation on titanium and its alloys, RSC Adv. 3 (2013) 19725–19743, https://doi.org/10.1039/c3ra43465f.

[14] K. Mediaswanti, C. Wen, E.P. Ivanova, C.C. Berndt, F. Malherbe, Vy Thi Hong Pham, J. Wang, A review on bioactive porous metallic biomaterials, J. Biomimetics, Biomaterials Tissue Eng. 18 (1) (2013) 1–8 https://doi.org/10.4172/1662-100X.1000104.

[15] H.T. Chen, H.Y. Shu, C.J. Chung, J.L. He, Assessment of bone morphogenic protein and hydroxyapatite–titanium dioxide composites for bone implant materials, Surf. Coat. Technol. 276 (2015) 168–174 https://doi.org/10.1016/j.surfcoat.2015.06.056.

[16] R.B. Heimann, Structure, properties, and biomedical performance of osteoconductive bioceramic coatings, Surf. Coat. Technol. 233 (2013) 27–38 https://doi.org/10.1016/j.surfcoat.2012.11.013.

[17] M. Geetha, A.K. Singh, R. Asokamani, A.K. Gogia, Ti based biomaterials, the ultimate choice for orthopaedic implants – a review, Prog. Mater. Sci. 54 (2009) 397–425, https://doi.org/10.1016/j.pmatsci.2008.06.004.

[18] A. Arifin, A.B. Sulong, N. Muhamad, J. Syarif, M.I. Ramli, Material processing of hydroxyapatite and titanium alloy (HA/Ti) composite as implant materials using powder metallurgy: a review, Mater. Des. 55 (2014) 165–175 https://doi.org/10.1016/j.matdes.2013.09.045.

[19] A. Mahapatro, Bio-functional nano-coatings on metallic biomaterials, Mater. Sci. Eng. C 55 (2015) 227–251 https://doi.org/10.1016/j.msec.2015.05.018.

[20] S. Bose, S. Tarafder, Calcium phosphate ceramic systems in growth factor and drug delivery for bone tissue engineering: a review, Acta Biomater. 8 (2012) 1401–1421, https://doi.org/10.1016/j.actbio.2011.11.017.

[21] Z. Sheikh, Yu L. Zhang, L. Grover, G.E. Merle, F. Tamimi, J. Barralet, In vitro degradation and in vivo resorption of dicalcium phosphate cement based grafts, Acta Biomater. 26 (2015) 338–346 https://doi.org/10.1016/j.actbio.2015.08.031.

[22] S.K. Sarkar, B.Y. Lee, A.R. Padalhin, A. Sarker, N. Carpena, B. Kim, K. Paul, H.J. Choi, S.H. Bae, B.T. Lee, Brushite-based calcium phosphate cement with multichannel hydroxyapatite granule loading for improved bone regeneration, J. Biomater. Appl. 30 (6) (2015) 823–837 https://doi.org/10.1177/0885328215601938.

[23] M.B. Sedelnikova, E.G. Komarova, Yu P. Sharkeev, T.V. Tolkacheva, V.V. Sheikin, V.S. Egorkin, D.V. Mashtalyar, A.A. Kazakbaeva, J. Schmidt, Characterization of the micro-arc coatings containing β-tricalcium phosphate particles on Mg-0.8Ca alloy, Metals 8 (4) (2018) 238 https://doi.org/10.3390/met8040238.

[24] S. Shadanbaz, G.J. Dias, Calcium phosphate coatings on magnesium alloys for biomedical applications: a review, Acta Biomater. 8 (2012) 20–30, https://doi.org/10.1016/j.actbio.2011.10.016.

[25] J.M. Bouler, P. Pilet, O. Gauthier, E. Verron, Biphasic calcium phosphate ceramics for bone reconstruction: a review of biological response, Acta Biomater. 53 (2017) 1–12 https://doi.org/10.1016/j.actbio.2017.01.076.

[26] G. Graziani, M. Bianchi, E. Sassoni, A. Russo, M. Marcacci, Ion-substituted calcium phosphate coatings deposited by plasmaassisted techniques: a review, Mater. Sci. Eng. C 74 (1) (2017) 219–229 https://doi.org/10.1016/j.msec.2016.12.018.

[27] S.S. Samandaria, K. Alamarab, S.S. Samandari, Calcium phosphate coatings: morphology, micro-structure and mechanical properties, Ceram. Int. 40 (2014) 563–572 https://doi.org/10.1016/j.ceramint.2013.06.038.

[28] C. Lindahl, W. Xia, H. Engqvist, A. Snis, J. Lausmaa, A. Palmquist, Biomimetic calcium phosphate coating of additively manufactured porous CoCr implants, Appl. Surf. Sci. 353 (2015) 40–47 https://doi.org/10.1016/j.apsusc.2015.06.056.

[29] R.I.M. Asri, W.S.W. Harun, M.A. Hassan, S.A.C. Ghani, Z. Buyong, A Review of hydroxyapatite-based coating techniques: sol-gel and electrochemical depositions on biocompatible metals, J. Mech. Behav. Biomed. Mater. 57 (2016) 95–108 https://doi.org/10.1016/j.jmbbm.2015.11.031.

[30] M. Catauro, F. Papale, L. Sapio, S. Naviglio, Biological influence of Ca/P ratio on calcium phosphate coatings by sol-gel processing, Mater. Sci. Eng. C 65 (2016) 188–193 https://doi.org/10.1016/j.msec.2016.03.110.

[31] K.A. Prosolov, K.S. Popova, O.A. Belyavskaya, J.V. Rau, K.A. Gross, A. Ubelis, Yu P. Sharkeev, RF magnetron-sputtered coatings deposited from biphasic calcium phosphate targets for biomedical implant applications, Bioactive Materials 2 (3) (2017) 170–176 https://doi.org/10.1016/j.bioactmat.2017.07.003.

[32] R.A. Surmenev, M.A. Surmeneva, K.E. Evdokimov, V.F. Pichugin, Thorsten Peitsch, M. Epple, Surf. Coat. Technol. 205 (2011) 3600–3606, https://doi.org/10.1016/j.surfcoat.2010.12.039.

[33] Yi Wang, H. Yu, C. Chen, Zh Zhao, Review of the biocompatibility of micro-arc oxidation coated titanium alloys, Mater. Des. 85 (2015) 640–652 https://doi.org/10.1016/j.matdes.2015.07.086.

[34] M. Rizwan, R. Alias, U. Zh Zaidi, R. Mahmoodian, M. Hamdi, Surface modification of valve metals using plasma electrolytic oxidation (PEO) for antibacterial applications: a review, J. Biomed. Mater. Res. A 106 (2) (2018) 590–605, https://doi.org/10.1002/jbm.a.36259.

[35] S.V. Dorozhkin, Calcium orthophosphate deposits: preparation, properties and biomedical applications, Mater. Sci. Eng. C 55 (2015) 272–326 https://doi.org/10.1016/j.msec.2015.05.033.

[36] M. Furko, Y. Jiang, T.A. Wilkins, C. Balázsi, Electrochemical and morphological investigation of silver and zinc modified calcium phosphate bioceramic coatings on metallic implant materials, Mater. Sci. Eng. C 62 (2016) 249–259 https://doi.org/10.1016/j.msec.2016.01.060.

[37] D. Campoccia, L. Montanaro, C.R. Arciola, A review of the biomaterials technologies for infection-resistant surfaces, Biomaterials 34 (2013) 8533–8554 https://doi.org/10.1016/j.biomaterials.2013.07.089.

[38] V. Stanić, D. Janaćković, S. Dimitrijević, S.B. Tanasković, M. Mitrić, M.S. Pavlović, A. Krstić, D. Jovanović, S. Raičević, Synthesis of antimicrobial monophase silver-doped hydroxyapatite nanopowders for bone tissue engineering, Appl. Surf. Sci. 257 (2011) 4510–4518, https://doi.org/10.1016/j.apsusc.2010.12.113.

[39] G. Madhumitha, G. Elango, S.M. Roopan, Bio-functionalized doped silver nanoparticles and its antimicrobial studies, J. Sol. Gel Sci. Technol. 72 (2015) 476–483, https://doi.org/10.1007/s10971-014-3591-2.
[40] G.A. Fielding, M. Roy, A. Bandyopadhyay, S. Bose, Antibacterial and biological characteristics of silver containing and strontium doped plasma sprayed hydroxyapatite coatings, Acta Biomater. 8 (2012) 3144–3152 https://doi.org/10.1016/j.actbio.2012.04.004.
[41] V. Kotharua, R. Nagumothua, C.B. Arumugamb, M. Veerappana, S. Sankaranc, M. Davoodbashad, T. Nooruddin, Fabrication of corrosion resistant, bioactive and antibacterial silver substituted hydroxyapatite/titania composite coating on Cp Ti, Ceram. Int. 38 (2012) 731–740, https://doi.org/10.1016/j.ceramint.2011.07.065.
[42] A.A. Ivanova, M.A. Surmeneva, I.Y. Grubova, A.A. Sharonova, V.F. Pichugin, M.V. Chaikina, V. Buck, O. Prymak, M. Epple, R.A. Surmenev, Influence of the substrate bias on the stoichiometry and structure of RF-magnetron sputter-deposited silvercontaining calcium phosphate coatings, Mat.-wiss. u. Werkstofftech. 44 (2–3) (2013) 218–225, https://doi.org/10.1002/mawe.201300101.
[43] L. Yin, Z. Fu, Y. Li, B. Liu, Z. Lin, J. Lu, X. Chen, X. Han, Y. Deng, W. Hu, D. Zou, C. Zhong, Enhanced antibacterial properties of biocompatible titanium *via* electrochemically deposited Ag/TiO_2 nanotubes and chitosan–gelatin–Ag–ZnO complex coating, RSC Adv. 9 (2019) 4521–4529, https://doi.org/10.1039/c8ra07682k.
[44] Y. Yan, J. Sun, Y. Han, D. Li, K. Cui, Microstructure and bioactivity of Ca, P and Sr doped TiO_2 coating formed on porous titanium by micro-arc oxidation, Surf. Coat. Technol. 205 (6) (2010) 1702–1713, https://doi.org/10.1016/j.surfcoat.2010.09.040.
[45] W. Liu, M. Cheng, T. Wahafu, Y. Zhao, H. Qin, J. Wang, X. Zhang, The in vitro and in vivo performance of a strontium-containing coating on the low-modulus Ti35Nb2Ta3Zr alloy formed by micro-arc oxidation, J. Mater. Sci. Mater. Med. 26 (2015) 203, https://doi.org/10.1007/s10856-015-5533-0.
[46] A.M. Pietak, J.W. Reid, M.J. Stott, M. Sayer, Silicon substitution in the calcium phosphate bioceramics, Biomaterials 28 (28) (2007) 4023–4032, https://doi.org/10.1016/j.biomaterials.2007.05.003.
[47] A. Rudawska, E. Jacniacka, Analysis for determining surface energy uncertainty by the Owens-Wendt method, Int. J. Adhesion Adhes. 4 (2009) 451–457 https://doi.org/10.1016/j.ijadhadh.2008.09.008.
[48] C.N. Martini, J.N. Brandani, M. Gabrielli, M.C. Vila, Effect of hexavalent chromium on proliferation and differentiation to adipocytes of 3T3-L1 fibroblasts, Toxicol. In Vitro 28 (14) (2014) 700–706 https://doi.org/10.1016/j.tiv.2014.02.003.
[49] J.P. Mather, P.E. Roberts, Introduction to Cell and Tissue Culture. Theory and Technique, Plenum Press, New York, 2002.
[50] O. Prymak, D. Bogdansk, S.A. Esenwein, M. Koller, M. Epple, NiTi shape memory alloys coated with calcium phosphate by plasma-spraying. Chemical and biological properties, Mat.-wiss. u. Werkstofftech. 35 (5) (2004) 346–351 https://doi.org/10.1002/mawe.200400753.
[51] S.V. Gnedenkov, YuP. Scharkeev, S.L. Sinebryukhov, O.A. Khrisanfova, E.V. Legostaeva, A.G. Zavidnaya, A.V. Puz, I.A. Khlusov, formation and properties of bioactive surface layers on titanium, Inorg. Mater.: Appl. Res. 2 (5) (2011) 474–481, https://doi.org/10.1134/S2075113311050133.
[52] I.A. Khlusov, Yu Dekhtyar, M.Yu Khlusova, E.A. Gostischev, YuP. Sharkeev, V.F. Pichugin, E.V. Legostaeva, Novel concepts of “Niche-Relief” and “Niche-Voltage” for stem cells as a base and hematopoietic tissues biomimetic engineering. International symposium on biomedical engineering and medical physics, IFMBE Proceedings. Riga, Latvia 38 (2012) 99–102 https://doi.org/10.1007/978-3-642-34197-7_26.
[53] M.B. Sedelnikova, E.G. Komarova, YuP. Sharkeev, A.V. Ugodchikova, L.S. Mushtovatova, M.R. Karpova, V.V. Sheikin, L.S. Litvinova, I.A. Khlusov, Antibacterial micro-arc coatings on Ti and Ti-40Nb alloy: characterization of the properties and behavior in synthetic biological media, Surf. Coat. Technol. 369 (2019) 52–68 https://doi.org/10.1016/j.surfcoat.2019.04.021.
[54] K. Nan, T. Wu, J. Chen, S. Jiang, Y. Huang, G. Pei, Strontium doped hydroxyapatite film formed by micro-arc oxidation, Mater. Sci. Eng. C 29 (2009) 1554–1558, https://doi.org/10.1016/j.msec.2008.12.018.
[55] D. Hu, K. Li, Y. Xie, H. Pan, J. Zhao, L. Huang, X. Zheng, Different response of osteoblastic cells to Mg^{2+}, Zn^{2+} and Sr^{2+} doped calcium silicate coatings, J. Mater. Sci. Mater. Med. 27 (2016) 56, https://doi.org/10.1007/s10856-016-5672-y.